



Carbon isotope ($\delta^{13}\text{C}$) excursions suggest times of major methane release during the last 14 kyr in Fram Strait, the deep-water gateway to the Arctic

C. Consolaro^{1,2}, T. L. Rasmussen¹, G. Panieri¹, J. Mienert¹, S. Bünz¹, and K. Sztybor¹

¹CAGE – Centre for Arctic Gas Hydrate, Environment and Climate, Department of Geology, UiT the Arctic University of Norway, Dramsveien 201, 9037 Tromsø, Norway

²School of Geography, Earth & Environmental Sciences, Plymouth University, Drake Circus, Plymouth PL4 8AA, UK

Correspondence to: C. Consolaro (chiara.consolaro@uit.no, chiara.consolaro@plymouth.ac.uk, chiara.consolaro@icloud.com)

Received: 16 September 2014 – Published in Clim. Past Discuss.: 24 October 2014

Revised: 18 March 2015 – Accepted: 27 March 2015 – Published: 17 April 2015

Abstract. We present results from a sediment core collected from a pockmark field on the Vestnesa Ridge ($\sim 80^\circ\text{N}$) in the eastern Fram Strait. This is the only deep-water gateway to the Arctic, and one of the northernmost marine gas hydrate provinces in the world. Eight ^{14}C AMS dates reveal a detailed chronology for the last 14 ka BP. The $\delta^{13}\text{C}$ record measured on the benthonic foraminiferal species *Cassidulina neoteretis* shows two distinct intervals with negative values termed carbon isotope excursion (CIE I and CIE II, respectively). The values were as low as -4.37‰ in CIE I, correlating with the Bølling–Allerød interstadials, and as low as -3.41‰ in CIE II, correlating with the early Holocene. In the Bølling–Allerød interstadials, the planktonic foraminifera also show negative values, probably indicating secondary methane-derived authigenic precipitation affecting the foraminiferal shells. After a cleaning procedure designed to remove authigenic carbonate coatings on benthonic foraminiferal tests from this event, the ^{13}C values are still negative (as low as -2.75‰). The CIE I and CIE II occurred during periods of ocean warming, sea-level rise and increased concentrations of methane (CH_4) in the atmosphere. CIEs with similar timing have been reported from other areas in the North Atlantic, suggesting a regional event. The trigger mechanisms for such regional events remain to be determined. We speculate that sea-level rise and seabed loading due to high sediment supply in combination with increased seismic activity as a result of rapid deglaciation may

have triggered the escape of significant amounts of methane to the seafloor and the water column above.

1 Introduction

Methane hydrate is an ice-like compound that exists in sediments at high pressures and low temperatures with sufficient supply of water and gas (Sloan, 1998). Methane hydrate provinces are widespread in the Arctic region, but their stability and longevity through time, and the significance of their contribution to the global carbon budget, are still poorly understood (e.g. Biastoch et al., 2011). The Arctic region is highly sensitive to climate change, and the effects of ongoing global warming are probably more extreme in the Arctic than elsewhere (e.g. Screen and Simmonds, 2010; Spielhagen et al., 2011). Recent discoveries suggest that the stability of gas hydrates in the Arctic Ocean in water depths up to about 400 m is already affected by ongoing ocean warming (e.g. Shakova et al., 2010; Ferré et al., 2012; Berndt et al., 2014). Methane emissions offshore west Svalbard from pockmarks in water depths greater than 800 m were recently recorded in the eastern part of the Vestnesa Ridge (Figs. 1 and 2), where several additional gas plumes were detected in 2010 (Bünz et al., 2012) and in 2012 (Smith et al., 2014), compared to the 2008 survey (Hustoft et al., 2009a), possibly indicating an increase in methane release activity. It is critical, therefore, to investigate the frequency of methane (CH_4)

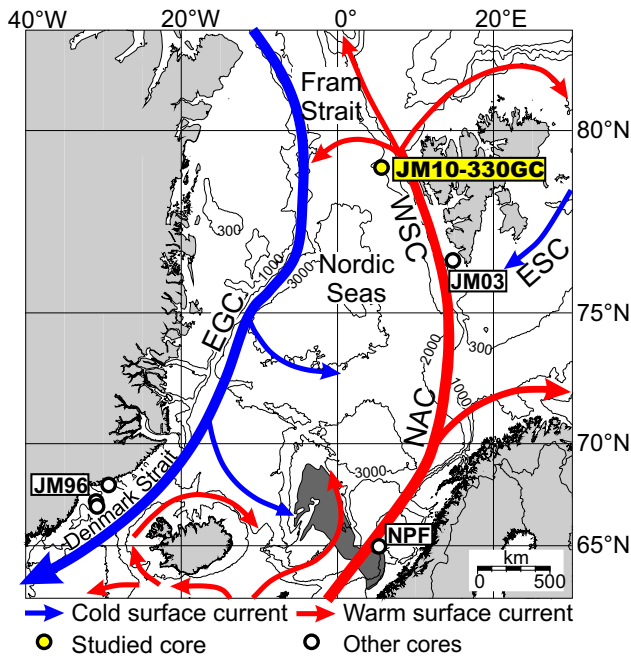


Figure 1. Bathymetric map of the Nordic Seas showing the major surface currents and the location of studied core JM10-330GC (yellow circle). Other cores are indicated with a white circle: JM96 cores are those described by Smith et al. (2001); JM03 represents core JM03-373PC2 used as reference core for the western Svalbard slope (Jessen et al., 2010); NPF cores are those described by Hill et al. (2012) in the Nyegga pockmark field next to the Storegga Slide (dark-grey area) on the mid-Norwegian margin. Abbreviations: NAC, North Atlantic Current; WSC, West Spitsbergen Current; ESC, East Spitsbergen Current; EGC, East Greenland Current.

emissions from the seafloor through time, especially in relation to past climate change and with a focus on periods of climate warming.

Gas hydrates occur in marine sediments along continental margins within a gas hydrate stability zone (GHSZ). The base of the GHSZ can be marked in seismic data by a bottom-simulating reflector (BSR) when sediments with free gas below and sediments with gas hydrate above this boundary are in contact, generating a negative acoustic impedance contrast (Shipley et al., 1979). Pockmarks are seafloor craters formed in soft, fine-grained sediments, where localized seepage of gas and pore fluid occurs (Judd and Hovland, 2007). The CH_4 originating from free gas below the BSR or released from gas hydrate dissociation may dissolve in pore waters, remain trapped as gas, or rise toward the seafloor as bubbles. In the near-seafloor sediments, up to 90% of the methane can be consumed by anaerobic oxidation of methane (AOM) according to Eq. (1): $\text{CH}_4 + \text{SO}_4^{2-} \rightarrow \text{HCO}_3^- + \text{HS}^- + \text{H}_2\text{O}$ by a consortium of methanotrophic archaea and sulfate-reducing bacteria within the sulfate–methane transition zone (SMTZ) (e.g. Barnes and Goldberg, 1976; Borowski et al., 1996; Boetius

et al., 2000; Hinrichs and Boetius, 2002; Treude et al., 2003; Reeburgh, 2007). The production of bicarbonate from AOM can induce the precipitation of calcium carbonate according to Eq. (2): $\text{Ca}^{2+} + 2\text{HCO}_3^- \rightarrow \text{CaCO}_3 + \text{CO}_2 + \text{H}_2\text{O}$. These so-called methane-derived authigenic carbonates can precipitate in different shapes like slabs, crusts, nodules, chimney, and pipes, with typical negative $\delta^{13}\text{C}$ values (e.g. Kulm and Suess, 1990; Greinert et al., 2001; Snyder et al., 2007). Benthonic foraminifera are often common in methane seep environments, and it has been demonstrated that their calcium carbonate tests can register the low $\delta^{13}\text{C}$ values of ambient dissolved inorganic carbon (DIC) derived from the oxidation of methane in the pore space of surrounding sediments (Wefter et al., 1994; Rathburn et al., 2003; Hill et al., 2004; Martin et al., 2004; Panieri et al., 2009, 2012, 2014a).

At high-flux seep sites the SMTZ is typically very shallow and methane may escape directly into the water column (Paull et al., 2005; Castellini et al., 2006). Most of the methane emitted at the seafloor is then consumed by methanotrophic aerobic microbes in the water column (Niemann et al., 2006; Reeburgh, 2007). For this reason planktonic foraminifera do not normally register the negative methane-derived $\delta^{13}\text{C}$ values in their tests. After deposition at the seafloor, both planktonic and benthonic foraminifera can be affected by alteration due to the precipitation of AOM-derived authigenic carbonates on their tests (Torres et al., 2003, 2010; Millo et al., 2005a; Panieri et al., 2009). In order to distinguish the isotopic records of the secondary overgrowth from the primary tests, it is necessary to repeat the isotopic analyses on specimens cleaned using a specific procedure designed to remove all authigenic carbonate coatings (Pena et al., 2008; Panieri et al., 2012, 2014b).

Here we present a detailed data analysis from a sediment core that was taken in a pockmark from the western part of the Vestnesa Ridge (Fig. 2). The core has been investigated for stable isotopes ($\delta^{18}\text{O}$ and $\delta^{13}\text{C}$), together with the distribution of planktonic foraminifera and sedimentological parameters, in order to reconstruct past changes in emission of methane in the area. Our results of the ^{14}C AMS (accelerator mass spectrometry) dates suggest an undisturbed sedimentary record for the last 14 kyr BP. Negative carbon isotope excursions (CIEs) during the Bølling–Allerød interstadials and during the early Holocene provide important records of past methane release events. This study is part of an ongoing research project at the Centre of Excellence for Arctic Gas Hydrate, Environment and Climate (CAGE) at the Arctic University of Norway, where different sediment cores from the Vestnesa Ridge pockmark field are being investigated in order to reconstruct past methane emissions from the seafloor (Panieri et al., 2014b).

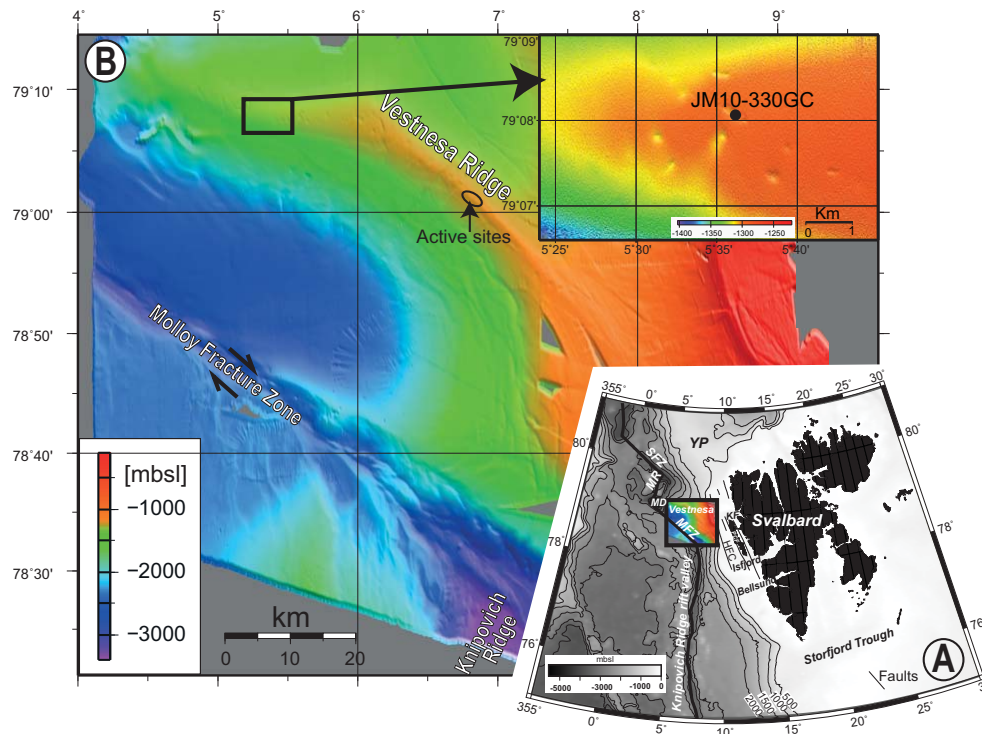


Figure 2. (a) Western Svalbard margin and eastern Fram Strait. Abbreviations: MFZ, Molloy Fracture Zone; MD, Molloy Deep; MR, Molloy Ridge; SFZ, Spitsbergen Fracture Zone; YP, Yermak Plateau. (b) Overview swath bathymetry map of the Vestnesa Ridge. Locations of studied core JM10-330GC and location of active sites with gas flares observed in June 2010 (Bünz et al., 2012) and in 2012 (Smith et al., 2014) are indicated. Figures are modified after Hustoft et al. (2009a).

2 Study Area

The Vestnesa Ridge is an elongated sediment drift at $\sim 80^\circ\text{N}$ at the northwestern Svalbard margin in the eastern Fram Strait. The Fram Strait is dominated by two main surface currents: the warm West Spitsbergen Current (WSC) and the cold East Greenland Current (EGC) (Aagaard et al., 1987) (Fig. 1). The WSC is the northernmost branch of the North Atlantic Current (NAC) and brings relatively warm, saline water along the western Svalbard margin and through the Fram Strait into the Arctic Ocean. This current is the major source of heat and salt to high northern latitudes and is very important for the generation of deep water in the Nordic Seas (Aagaard et al., 1985). The warm Atlantic water overlies the Greenland Sea Intermediate Water, which is generated from convection in the Nordic Seas (Aagaard et al., 1987). The EGC carries cold polar water and sea ice from the Arctic Ocean southwards along the East Greenland margin through the Denmark Strait and into the North Atlantic Ocean (Fig. 1).

The Vestnesa Ridge is located on hot, thin and young ($< 20\text{ Ma}$) oceanic crust (e.g. Hustoft et al., 2009a) (Fig. 2a and b). It belongs to the eastern-spreading segment of the Molloy Fracture Zone that is connected to the northernmost extension of the Mid-Atlantic Ridge system: the ultra-slow-

spreading Knipovich Ridge (Engen et al., 2008; Hustoft et al., 2009a) (Fig. 2a). The sediment crest of the Vestnesa Ridge is pierced with pockmarks (Fig. 2b) (e.g. Vogt et al., 1994; Hustoft et al., 2009a), and seismic data show a BSR 160–180 m beneath the seabed, indicating the presence of gas hydrate (Hustoft et al., 2009a; Petersen et al., 2010; Bünz et al., 2012). Active gas venting has recently been observed in the eastern part of the ridge, where thermogenic free gas migrates to the crest of the BSR anticline and further upward to the Vestnesa Ridge pockmark field (Hustoft et al., 2009a; Bünz et al., 2012; Smith et al., 2014). Seismic data beneath the pockmark field show vertical gas migration pathways (chimneys) that form conduits allowing the gas to bypass the hydrate stability zone (HSZ) and escape from the seafloor (Bünz et al., 2012). The pockmark fields in the deeper (1300 m water depth), western part of the ridge are most probably inactive, because no acoustic gas flares have been observed so far (Bünz et al., 2012).

3 Material and methods

Gravity core JM10-330GC (79.13°N , 5.6°E ; 420 cm long) was collected from about 1300 m water depth (mwd) in a pockmark located on the inactive western part of the Vestnesa Ridge (Figs. 1 and 2b). Before opening the core, mag-

netic susceptibility was measured with a Bartington MS2 loop sensor (Fig. 3). Afterwards the core was split longitudinally, and one half was X-rayed and then colour-imaged with a Jai L-107CC 3 CCD RGB line scan camera installed on an Avaatech XRF core scanner (Fig. 3). The other half was sampled at 5 cm intervals in 1 cm thick slices, weighed and subsequently freeze-dried. Dry samples were weighed and wet-sieved over mesh sizes of 63 μm , 100 μm and 1 mm. The residues were dried at 40 $^{\circ}\text{C}$. Benthonic and planktonic foraminifera were picked from the > 100 μm size fraction, counted (at least 300 specimens for each sample when possible) and identified to species level for assemblage analysis. In this paper, we only present data on the two most dominant planktonic species, *Neogloboquadrina pachyderma* sinistral (s) and *Turborotalita quinqueloba*, which together constitute 88–98 % of the assemblage. Ice-rafted detritus (IRD) was counted in the > 1 mm size fraction (Fig. 3).

Eight ^{14}C AMS dates were performed on monospecific samples of *N. pachyderma* (s) (Table 1) at the Chrono Centre of Queen's University, Belfast, UK. The radiocarbon dates were calibrated to calendar years using the Calib 7.0 program (Stuiver et al., 2014) and the marine calibration curve Marine13 (Reimer et al., 2013), which operates with a standard reservoir correction of -400 years (Mangerud and Gulliksen, 1975). A regional correction of $\Delta R = 7 \pm 11$ years was applied, following the recommendations for planktonic foraminiferal dates by Bondevik and Gulliksen (in Mangerud et al., 2006). The ages were calculated as the mid-point value from the calibrated age range ($\pm 2\sigma$). Calibrated dates are presented in years before present (BP; before AD 1950) with standard deviation of 2σ . The age model was constructed assuming linear sedimentation between the calibrated dates (Fig. 3). The reservoir effect is probably not constant through time, and especially during the Younger Dryas it was probably larger (e.g. Bard et al., 1994; Bondevik et al., 2006; Austin et al., 2011). However, the comparison of the stratigraphy and the magnetic susceptibility data between core JM10-330GC and core JM03-373PC2 (Fig. 1), which has been used as reference core for the western Svalbard slope (Jessen et al., 2010), indicates that a standard reservoir correction age is appropriate. In particular, the presence of a diatom-rich layer that was attributed to the early Holocene by Jessen et al. (2010), together with a marked shift in the species composition of the planktonic foraminiferal assemblage (previously dominated by the polar species *N. pachyderma* (s) and subsequently by the subpolar species *T. quinqueloba*), as well as the decrease in oxygen isotope values in the same interval, confirms an early Holocene age for these events, in accordance with our age model (Fig. 4).

Stable isotopes (oxygen and carbon; Table S1 in the Supplement) were measured on the planktonic foraminifera species *N. pachyderma* (s) and on the benthonic species *Cassidulina neoteretis* both picked from the > 100 μm size fraction. Stable isotopes were performed at the Leibniz Laboratory for Radiometric Dating and Isotope Research in Kiel,

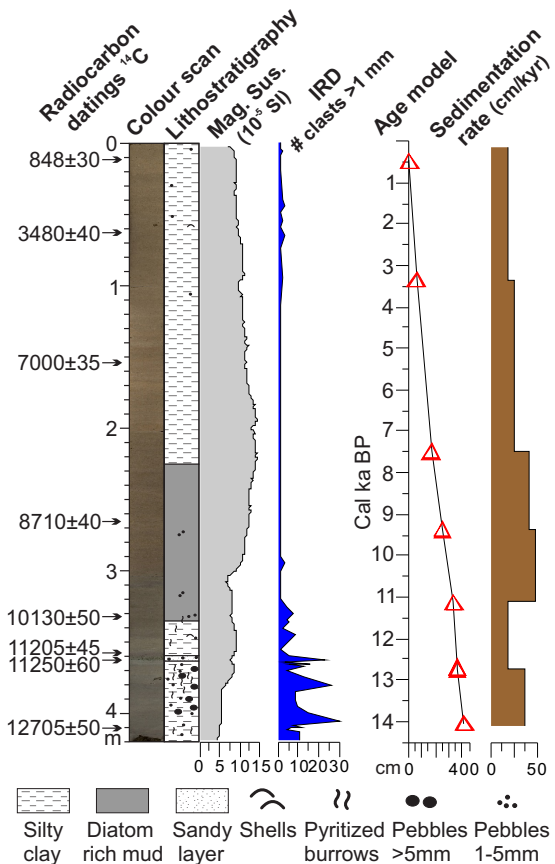


Figure 3. Left: lithology and colour scan of core JM10-330GC, together with magnetic susceptibility and concentration of ice-rafted debris (IRD) per gram dry weight sediment. Arrows indicate positions of original radiocarbon dates. Right: age model and calculated sediment accumulation rates. Red triangles indicate radiocarbon dates.

Germany, using a Finnigan MAT-253 mass spectrometer with a Kiel IV system (analytical precision of ± 0.05 ‰ for $\delta^{13}\text{C}$ and ± 0.1 ‰ for $\delta^{18}\text{O}$ estimated by measuring the certified standard NBS-19). All isotope results are reported in standard delta notation relative to Vienna Pee Dee Belemnite (VPDB). The $\delta^{18}\text{O}$ isotopic values were corrected for the ice volume effect ($\delta^{18}\text{O}_{\text{IVC}}$) using the Fairbanks (1989) sea-level curve as dated by Bard (1990) with a correction of 0.11 ‰ $\delta^{18}\text{O}$ per 10 m sea-level change (subtracted from the measured $\delta^{18}\text{O}$ values; Table S1).

Additional stable isotope analyses of cleaned benthonic foraminifera samples from the lower part of the core (418–370 cm) were performed on a Thermo Finnigan MAT252 mass spectrometer coupled with a CarboKiel-II carbonate preparation device (analytical precision ± 0.03 ‰ for $\delta^{13}\text{C}$ and ± 0.08 ‰ for $\delta^{18}\text{O}$ estimated by measuring the certified standard NBS-19; results are reported in standard delta notation relative to VPDB) at the Serveis Científic-Tècnics of the University of Barcelona (Table S1; Fig. 5). The benthonic

Table 1. Radiocarbon data and sedimentation rate ^a.

Depth (cm bsf)	Dated material	Laboratory reference	AMS ¹⁴ C dates (years BP)	Calibrated age cal years BP, $\pm 2\sigma$ median)	$\delta^{13}\text{C}$ (‰)	Sed. rate (cm kyr ⁻¹)
5–7	<i>N. pachyderma</i> (s)	UBA-19355	848 \pm 29	470 \pm 50	-1.2	18.75
60–61	<i>N. pachyderma</i> (s)	UBA-18143	3477 \pm 36	3340 \pm 100	-1.6	18.82
170–171	<i>N. pachyderma</i> (s)	UBA-19356	7001 \pm 33	7490 \pm 70	-1.1	26.51
250–251	<i>N. pachyderma</i> (s)	UBA-18144	8707 \pm 39	9370 \pm 100	-0.6	42.55
335–337	<i>N. pachyderma</i> (s)	UBA-19357	10 130 \pm 47	11 110 \pm 130	-0.7	49.43
360–361	<i>N. pachyderma</i> (s)	UBA-18145	11 203 \pm 45	12 690 \pm 110	-1.3	17.85
363–367	<i>N. pachyderma</i> (s)	UBA-19358	11 250 \pm 57	12 735 \pm 130	-1.5	17.85
413–418	<i>N. pachyderma</i> (s)	UBA-18146	12 575 \pm 51	14 040 \pm 150	-1.1	38.32

^a Radiocarbon data and calibrated ages in core JM10-330GC together with the calculated linear sedimentation rate.

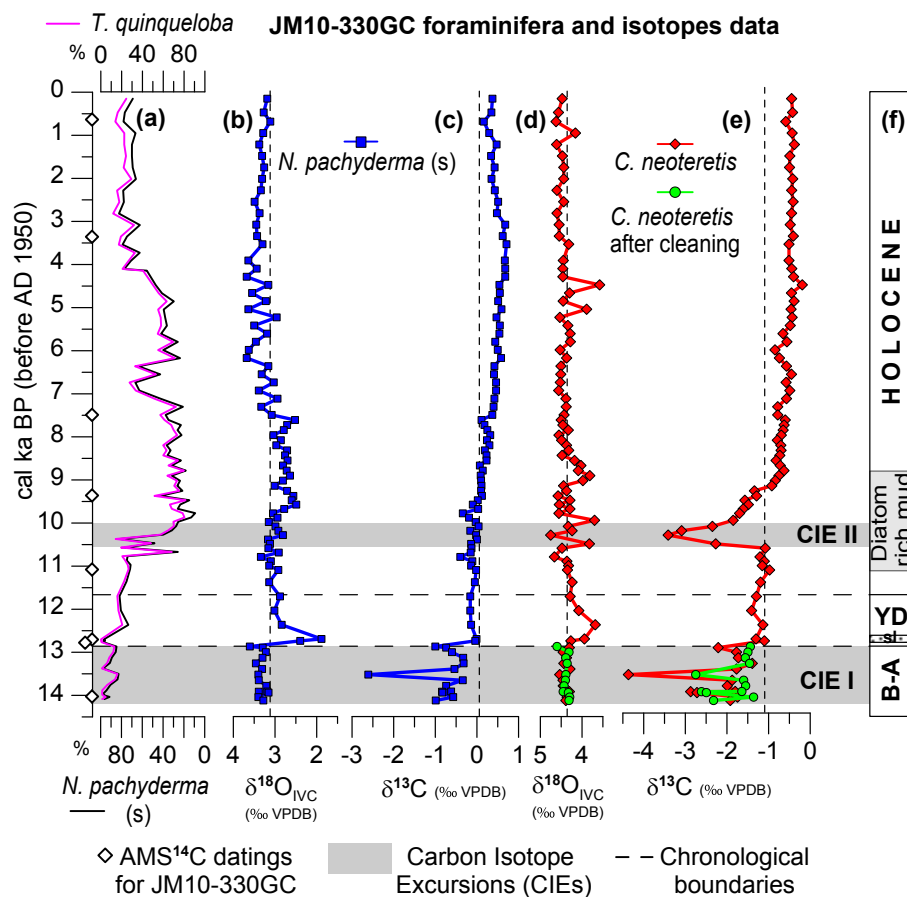


Figure 4. Planktonic foraminifera and geochemical data of core JM10-330GC plotted versus calibrated (cal) ka before present (BP; before AD 1950): (a) relative abundance of *Neogloboquadrina pachyderma* (s) (black line) and *Turborotalita quinqueloba* (purple line), (b) ice-volume-corrected (IVC) $\delta^{18}\text{O}_{\text{IVC}}$ record of *N. pachyderma* (s), (c) $\delta^{13}\text{C}$ record of *N. pachyderma* (s), (d) $\delta^{18}\text{O}_{\text{IVC}}$ record of *Cassidulina neoteretis* before (red line) and after (green line) the cleaning protocol of Pena et al. (2005), (e) $\delta^{13}\text{C}$ record of *C. neoteretis* before (red line) and after (green line) the cleaning protocol of Pena et al. (2005), and (f) stratigraphy obtained for JM10-330GC with chronological subdivisions (dashed lines). Dotted vertical lines indicate average core values. White diamonds on the y axis indicate AMS ¹⁴C dating points for JM10-330GC. Shaded horizontal bars indicate carbon isotope excursion (CIE) I and II. Abbreviations: B-A, Bølling–Allerød; YD, Younger Dryas; sl, sandy layer.

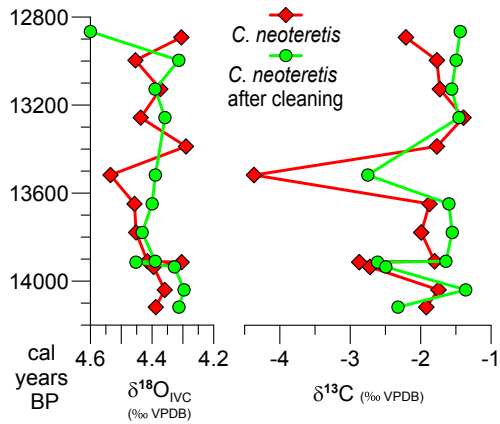


Figure 5. Detail of the $\delta^{18}\text{O}$ and $\delta^{13}\text{C}$ record of *C. neoteretis* from CIE I interval, before (red line) and after (green line) the cleaning protocol of Pena et al. (2005).

foraminiferal samples were cleaned following the protocol of Pena et al. (2005), which is adapted from Boyle and Rosenthal (1996). Prior to cleaning, the foraminifera were gently crushed between clean glass plates to break open individual chambers. The cleaning steps comprise (1) removal of clays, manganese–iron oxides and other mineral phases by a reductive cleaning step; (2) oxidative cleaning to eliminate organic matter; and (3) weak acid leaching to remove remaining impurities from the shell surfaces. This protocol has proven to be efficient in removing the diagenetic carbonates attached to the tests of foraminifera (Pena et al., 2008; Panieri et al., 2012, 2014b).

The preservation states of the foraminifera tests were examined by scanning electron microscope (SEM) in order to identify presence of secondary overgrowth of methane-derived authigenic carbonates in selected representative specimens of *N. pachyderma* (s) and *C. neoteretis* before the cleaning procedure (Figs. 6 and 8). Qualitative estimates of the trace metal content were obtained from the test surface (coated with gold/palladium) with energy dispersive X-ray spectroscopy (EDS) (Fig. 7). SEM secondary electronic images and EDS spectra were acquired on a JEOL 6610 tungsten SEM equipped with an Oxford Instruments AzTEC EDS system at the Electron Microscopy Centre, Plymouth University, UK.

4 Results

4.1 Chronology and lithology

Based on the calibrated ^{14}C dates, the distribution patterns of polar and subpolar planktonic foraminifera species (Fig. 4a), and the benthonic and planktonic $\delta^{18}\text{O}$ records (Fig. 4b–d), we have correlated core JM10-330GC to the Greenland ice core event stratigraphy, applying the new Greenland Ice Core Chronology 2005 (GICC05) of Rasmussen et al. (2006). The

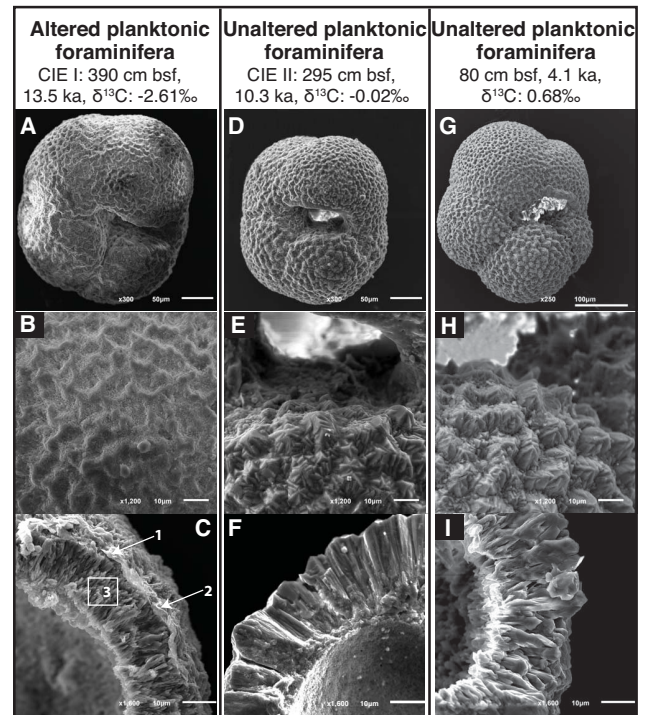


Figure 6. Representative SEM images of uncleaned *N. pachyderma* (s) specimens from different intervals: (a, b, c) from 390 cm bsf, (d, e, f) from 295 cm bsf, and (g, h, i) from 80 cm bsf. (a) *N. pachyderma* (s) test from the most depleted interval within CIE I ($\delta^{13}\text{C}$: -2.61‰ , 13.5 ka, 390 cm bsf) showing a test with surface alteration. (b) Detail of picture (a) with clearly altered external surface. (c) Broken test of a different specimen of *N. pachyderma* (s) from the same interval, where a thin deposited layer (methane-derived coating) unevenly covers the external text, whereas the foraminiferal wall shows a pristine structure with pristine crystal palisades. The numbers in the picture indicate EDS analyses in Fig. 7. (d) *N. pachyderma* (s) from CIE II interval ($\delta^{13}\text{C}$: -0.02‰ , 10.3 ka, 295 cm bsf) showing an unaltered test. (e) Detail of picture (d) with pristine shell structure. (f) Detail of the wall structure with pristine crystal palisades from a different specimen in the same interval. (g) *N. pachyderma* (s) from interval with normal ^{13}C values ($\delta^{13}\text{C}$: 0.68‰ , 4.1 ka, 80 cm bsf) showing a well-preserved test with pristine shell structure. (h) Detail of picture (g) with pristine crystals shape. (i) Detail of the wall structure with pristine crystal palisades from a different specimen in the same interval. Picture magnifications and length of the white bar are indicated in each picture.

GICC05 timescale is b2k (before AD 2000); therefore to compare it with the calendar ages (before AD 1950) used in this paper, we have subtracted 50 years from the GICC05 timescale. In this new chronology the different periods are defined as follows: end of the Bølling interstadial, 14.025 ka; onset of the Younger Dryas (YD) stadial, 12.85 ka; YD–Holocene transition, 11.65 ka.

Our age model shows that the core contains postglacial sediments covering the last 14 kyr, spanning from the upper

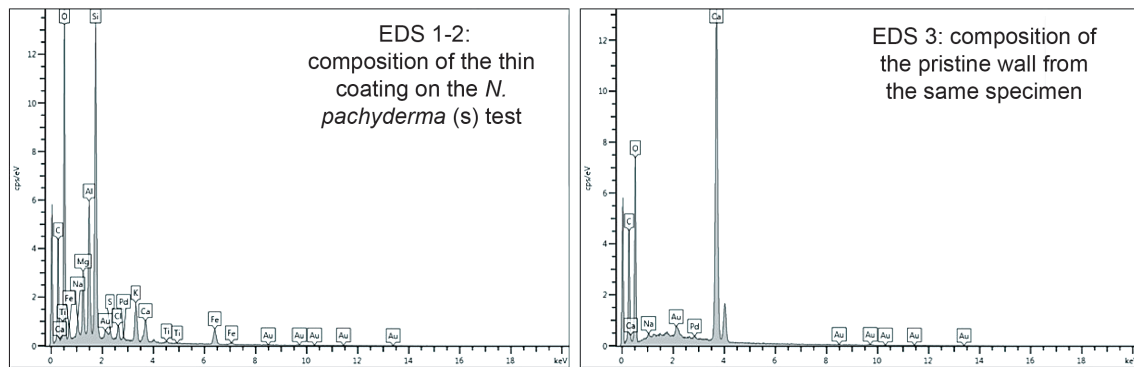


Figure 7. Left panel, EDS 1–2: energy dispersive X-ray spectroscopy (EDS) spectra of outer layer on the test of *N. pachyderma* (s) from the most depleted interval within CIE I (Fig. 6c) showing enrichments in Si and Mg and traces of Fe and S. Right panel, EDS 3: EDS spectra of the internal part of the wall of the same specimens (Fig. 6c) showing a pristine composition consisting of CaCO_3 .

part of the Bølling–Allerød (B-A) interstadial periods to the Holocene (Fig. 4). The lithology (Fig. 3) is very similar to the reference core of the western Svalbard slope (Jessen et al., 2010), with the lower part (418–335 cm; 14.1–11.1 ka; B-A and YD interval) characterized by a high concentration of ice-rafted debris (IRD) and common pyritized burrows indicative of bioturbation, with a greenish sandy layer at the beginning of the YD (360 cm; 12.7 ka). There is a fine-grained, structureless, silty mud interval with a high abundance of diatoms in the middle part (335–225 cm; 11.1–8.8 ka, labelled diatom-rich mud in Fig. 4f). A homogeneous hemipelagic, grey clay with a very low amount of IRD is present in the upper interval (225–0 cm; 8.8 ka to present).

The sedimentation rate is higher during the B-A period ($\sim 38 \text{ cm kyr}^{-1}$) and in the early Holocene ($42\text{--}50 \text{ cm kyr}^{-1}$) but lower during the Younger Dryas (YD: $\sim 18 \text{ cm kyr}^{-1}$) and after 7.5 ka ($19\text{--}26 \text{ cm kyr}^{-1}$) (Fig. 3; Table 1).

4.2 Carbon isotope excursions (CIEs)

During the Bølling–Allerød interstadials, the $\delta^{13}\text{C}$ record of the infaunal benthonic foraminifera *C. neoteretis* shows values considerably lower than the average core value of -1.10‰ (CIE I). The low values occur at about 13.9 (-2.87‰) and at 13.5 ka (-4.37‰), and there is another, less pronounced excursion at 12.9 ka (-2.21‰ ; Fig. 4e). This first interval with depleted $\delta^{13}\text{C}$ has been termed carbon isotope excursion I (CIE I). The stable isotope analyses were repeated for this interval on *C. neoteretis* specimens cleaned with a procedure designed to remove authigenic carbonate coatings (Pena et al., 2008; Panieri et al., 2012, 2014b). The $\delta^{13}\text{C}$ values obtained are higher (by up to 1.6‰) compared to the tests cleaned with the standard protocol, but are still lower (as low as -2.75‰) than the average value of the record (-1.10‰) (Table S1; Fig. 5).

The planktonic $\delta^{13}\text{C}$ values during the CIE I interval are lower than the average core value of 0.07‰ and show one prominent excursion (-2.61‰) at 13.5 ka (Fig. 4c).

Another interval with low benthonic $\delta^{13}\text{C}$ values occurs in the early part of the Holocene (CIE II; Fig. 4e). This event lasted approximately 500 years (ca. 10.5–10 ka) and is characterized by benthonic $\delta^{13}\text{C}$ values that are lower than -2‰ , with the most prominent excursion at 10.3 ka (-3.41‰). CIE II is not recorded in the planktonic record, where the $\delta^{13}\text{C}$ values are very close to the average core value and within the normal range of the marine environment (Fig. 4c).

The $\delta^{13}\text{C}$ values in both benthonic and planktonic records between the two events (from about 12.8 to 10.5 ka) are very close or slightly lower than average values, whereas after 9 ka they are higher compared to the average values (Fig. 4c–e).

The $\delta^{18}\text{O}_{\text{IVC}}$ benthonic and planktonic records present little variability if compared to the average values of 4.35 and 3.12‰ , respectively (Fig. 4b and d). Light isotope excursions are present in both the benthonic ($<0.7\text{‰}$ more depleted than the average) and planktonic record (about 1.2‰ more depleted than the average) during the Younger Dryas and are probably related to a melt water event, which is also documented by a sandy layer (Fig. 4f). No negative oxygen isotope excursions are associated with CIE I, and in the early Holocene only two relatively light ($<0.7\text{‰}$ more depleted than the average) excursions exist in the $\delta^{18}\text{O}$ benthonic record at the beginning and at the end of CIE II (Fig. 4d).

The SEM images of *N. pachyderma* (s) from the most negative excursion of CIE I (-2.61‰ , 390 cm bsf (below seafloor) at 13.5 ka) show evidence of surface alteration (Fig. 6a–b) with a thin coating ($<1 \mu\text{m}$) unevenly covering parts of the test (Fig. 6c). The EDS estimates show that the deposited layer is highly enriched in Si and moderately enriched in Mg, with minor traces of Fe and S (EDS 1 and 2 in Figs. 6c and 7). The internal part of the wall looks unaltered, with pristine crystal palisades consisting of CaCO_3 (EDS 3 in Figs. 6c and 7).

The *N. pachyderma* (s) tests from CIE II (-0.02‰ , 295 cm bsf at 10.3 ka) and from the late Holocene (0.68‰ , 80 cm bsf at 4.1 ka) are well preserved, with pristine shell

structure (Fig. 6d–e and g–h) and walls characterized by crystal palisades typical of this species (Fig. 6f–i).

The SEM images of *C. neoteretis* (uncleaned specimens) are more difficult to interpret. No clear coatings were detected on the test surface of the specimens from both depleted intervals, CIE I ($\delta^{13}\text{C}$: -4.37‰ , 13.5 ka, 390 cm bsf; Fig. 8a–c) and CIE II ($\delta^{13}\text{C}$: -3.41‰ , 10.3 ka, 295 cm bsf; Fig. 8d–f). In both cases, the surface of the tests appears altered with enlarged and irregular pores, probably due to dissolution and possibly associated with recrystallization in the internal part of the test. The specimens from CIE II look even more altered compared to the ones from CIE I. Specimens of *C. neoteretis* were very rare in this interval and almost all the specimens have been used for isotope analyses. The specimens used for the SEM pictures were the only examples left and were very small (note the scale in Fig. 8c) and very poorly preserved.

The *C. neoteretis* tests from an interval with normal ^{13}C values (-0.44‰ , 80 cm bsf at 4.1 ka) are well preserved, with pristine shell structure and small ($<1\mu\text{m}$), round pores (Fig. 8g–i).

5 Discussion

5.1 CIEs: secondary overgrowth vs. primary tests

The benthonic foraminiferal (*C. neoteretis*) $\delta^{13}\text{C}$ record shows negative excursions in the Bølling–Allerød interstadials (CIE I) and in the early Holocene (CIE II). These values are 1–3.3‰ lower than the average value of -1.10‰ in the sediment core, which is comparable to values of *C. neoteretis* recovered from sites unaffected by methane seepage from the same region (ca. -1 to 0‰ in the northern Barents Sea: Woltenburg et al., 2001; -1.15‰ in a control site away from the Håkon Mosby mud volcano in the Barents Sea: Mackensen et al., 2006).

The planktonic foraminiferal $\delta^{13}\text{C}$ record shows a similar negative trend only during CIE I, with one prominent negative excursion (-2.61‰) at 13.5 ka (Fig. 4c). Here the planktonic values are generally lower compared to the normal $\delta^{13}\text{C}$ range of *N. pachyderma* (s) in the same region (between ca. -0.5 and 1‰ : Volkman and Mensch, 2001; Nørgaard-Pedersen et al., 2003; Sarnthein et al., 2003; Jessen et al., 2010).

Planktonic foraminifera are not expected to record a signal from methane in the water column, because most of the methane that has escaped from the seafloor should be consumed by methanotrophic bacteria in the sediment and water column (Dickens, 2001; Reeburgh, 2007). The negative values of *N. pachyderma* (s) can be attributed to diagenetic alteration that may stem from methane-derived authigenic carbonates on the foraminiferal tests after their deposition to the seafloor (Torres et al., 2003, 2010; Millo et al., 2005a; Panieri et al., 2009).

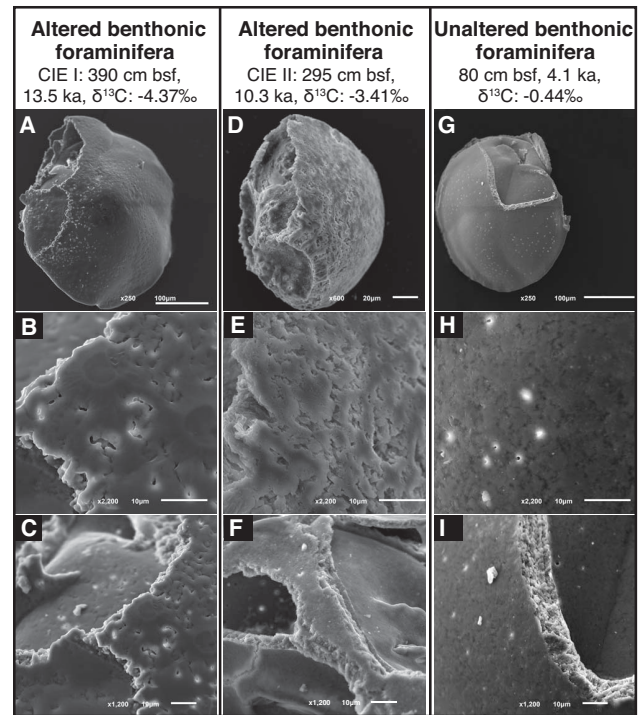


Figure 8. Representative SEM images of uncleaned *C. neoteretis* specimens from the depleted intervals (a–c, from 390 cm bsf; d–f, from 295 cm bsf) and from an interval with normal ^{13}C values (g–i, from 80 cm bsf). (a) *C. neoteretis* test from the most depleted interval within CIE I ($\delta^{13}\text{C}$: -4.37‰ , 13.5 ka, 390 cm bsf) showing a test with surface alteration by dissolution features. (b) Detail of picture (a) where the external test shows enlarged pores ($5\text{--}7\mu\text{m}$) with irregular shapes. (c) Detail of picture (a) with a different magnification showing the irregular profile of the test wall. (d) *C. neoteretis* from CIE II interval ($\delta^{13}\text{C}$: -3.41‰ , 10.3 ka, 295 cm bsf) showing a test with surface alteration characterized by dissolution features. Note the smaller scale of the picture. (e) Detail of picture (d) where the enlarged and irregular shaped pores are widespread. (f) Detail of the test of a different specimen from the same interval where the surface alteration is less evident but the profile of the test walls is quite irregular. (g) *C. neoteretis* from an interval with normal ^{13}C values ($\delta^{13}\text{C}$: -0.44‰ , 4.1 ka, 80 cm bsf) showing a well-preserved test with pristine shell structure. (h) Detail of picture (g) showing small ($<1\mu\text{m}$) and round-shaped pores with no alteration features. (i) Detail of picture (g) with a different magnification showing a well-preserved test and regular profile of the test wall. Picture magnifications and length of the white bar are indicated in each picture.

Therefore, in order to distinguish the isotopic records of the secondary overgrowth from the primary tests, we repeated the isotopic analyses on cleaned *C. neoteretis* specimens from the CIE I interval (see above). The repetition of the isotopic analyses for *N. pachyderma* (s) and for *C. neoteretis* from the CIE II interval was impossible due to a lack of material. Thus a detailed SEM investigation was carried out on both species (see below).

The $\delta^{13}\text{C}$ values obtained after the cleaning procedure (as low as -2.75‰) are still significantly lower than the core average (-1.10‰ ; Table S1; Fig. 5) and also lower compared to the $\delta^{13}\text{C}$ records of *C. neoteretis* of the last deglaciation from the same region, with values ca. -0.5 to 0.3‰ in the Kara Sea (Lubinski et al., 2001), ca. -1 to 0‰ in the northern Barents Sea (Wollenburg et al., 2001) and ca. 0 to 1.5‰ in the southwestern Barents Sea (Aagaard-Sørensen et al., 2010). Dead specimens (empty tests) of *C. neoteretis* from surface samples at the active Håkon Mosby mud volcano in the Barents Sea show very similar $\delta^{13}\text{C}$ negative values (from -1.65 to -2.82‰) (Mackensen et al., 2006). We suggest that the low $\delta^{13}\text{C}$ values obtained after the cleaning procedure could be the result of calcification in the presence of ^{13}C -depleted DIC and probably ingestion of ^{13}C -depleted methanotrophic microbes on which foraminifera feed (e.g. Rathburn et al., 2003; Hill et al., 2004; Panieri et al., 2014a). We interpret the ^{13}C -depleted values of diagenetic overgrowth on the *C. neoteretis* shells as cumulatively added to the already negative values of the primary tests.

The SEM pictures of *N. pachyderma* (s) from the most negative excursion during CIE I (390 cm, 13.5 ka) show clear evidence of surface alteration with a thin coating enriched in SiO_2 , Mg and traces of FeS (Figs. 6c and 7). Authigenic silica is common in ancient limestones from seep sites (Smrzka et al., 2015), and similar SiO_2 enrichments have been observed in secondary coatings on *N. pachyderma* (s) from depleted ^{13}C intervals in the southwestern Greenland Sea (Millo et al., 2005a). The precipitation of silica phases would occur after AOM-derived mineral phases ceased to form but before the precipitation of late diagenetic calcite cements (Kuechler et al., 2012; Smrzka et al., 2015). Enrichments in Mg in the foraminiferal tests are typical of methane-derived authigenic carbonates, as previously observed by Torres et al. (2003, 2010). The production of bicarbonate and hydrogen sulfide increases carbonate alkalinity at the SMTZ, inducing the precipitation of carbonate minerals and pyrite (e.g. Ritger et al., 1987; Peckmann et al., 2001; Sassen et al., 2004).

N. pachyderma (s) in the early Holocene (CIE II) exhibit values in the normal marine range ($> -0.5\text{‰}$), and the tests from this interval do not show any sign of surface alteration or coatings (Fig. 6d–f).

No clear indications of coatings have been observed on the benthonic foraminiferal tests from both depleted intervals (CIE I and CIE II; Fig. 8a–f). The surface alteration in this case mainly consists of dissolution features, probably due to an increase in CO_2 during AOM in marine sediments (Eq. 2). It is also possible that the precipitation of methane-derived authigenic carbonates in this case has occurred inside the benthonic tests. This is probably because the smooth and imperforate test of *C. neoteretis* is less likely to accommodate contamination and crystalline overgrowth than the *N. pachyderma* (s) test with higher porosity and surface area, as already observed by Cook et al. (2011).

The results of the repeated isotope analyses on the cleaned specimens from CIE I interval seem to support this hypothesis since the cleaning procedure is meant to remove the authigenic carbonate overgrowth and the values obtained are indeed less negative compared to the uncleaned specimens. However, these aspects are not fully understood and require additional analyses and investigations.

5.2 CIEs: evidence for methane release

In order to explain the different results found for CIE I and CIE II, we have used a schematic diagram modified after Borowski et al. (1996) and suggest two different scenarios depending on the strength of the methane flux at the seep site (Fig. 9).

The intensity of upward methane flux can control sulfate (SO_4^{2-}) profiles and depth of the sulfate methane transition zone (SMTZ) if the sulfate diffusion from the seawater into the sediment and the sediment characteristics are considered constant (Fig. 9b).

The first scenario (Fig. 9a) represents CIE II, where only benthonic foraminifera show negative $\delta^{13}\text{C}$ values. In this case the methane flux is high and the SMTZ is very close to the seafloor. The oxidation of methane is less efficient, causing lower rates of AOM and higher methane flux into the bottom waters. The methane that escapes is then partially oxidized by methanotrophic aerobic microbes in the water column (Niemann et al., 2006). In this scenario, the negative $\delta^{13}\text{C}$ values in the benthonic foraminiferal tests are likely to be the result of calcification in the presence of ^{13}C -depleted DIC and probably ingestion of ^{13}C -depleted methanotrophic bacteria. In high advective flow settings, the surface communities are often dominated by bacterial mats (Treude et al., 2003; Boetius and Wenzhöfer, 2013) on which benthonic foraminifera can prey (Rathburn et al., 2003; Panieri et al., 2014a). Similar negative ^{13}C values (from -1.5 to -4.0‰) have been previously observed in benthonic foraminifera living at methane seep sites (Sen Gupta and Aharon, 1994; Weyer et al., 1994; Sen Gupta et al., 1997; Keigwin, 2002; Hill et al., 2003, 2004; Rathburn et al., 2003; Martin et al., 2007, 2010; Panieri et al., 2009, 2012, 2014a). However, we cannot exclude precipitation of early authigenic carbonates on the foraminiferal tests when they were still alive, as a product of AOM near the seafloor (e.g. Bohrmann et al. 1998).

The second scenario (Fig. 9c) represents CIE I, where both benthonic and planktonic foraminifera exhibit negative values of $\delta^{13}\text{C}$. We interpreted these anomalies in $\delta^{13}\text{C}$ as being due to secondary carbonate precipitation after the benthonic and planktonic foraminifera were buried. The precipitation of carbonate occurs when the pore water is oversaturated with respect to carbonate minerals. The SMTZ is typically a narrow zone of just a few centimetres (e.g. Iversen and Jørgensen, 1985; Niewöhner et al., 1998; Treude et al., 2005) resulting in the sharp negative shift in $\delta^{13}\text{C}$ recorded by both benthonic and planktonic foraminifera (see Figs. 4 and 5).

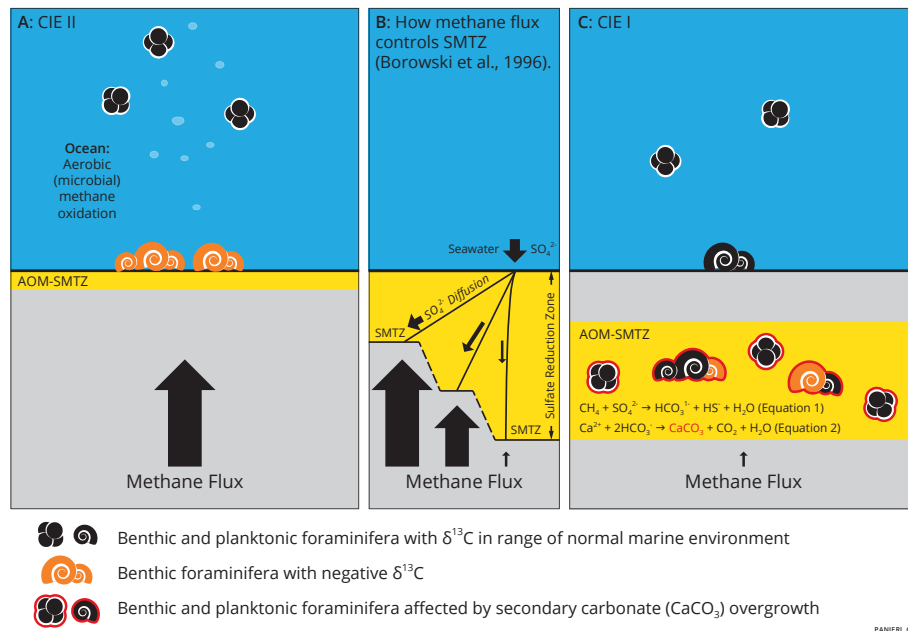


Figure 9. (a) Schematic diagram representing CIE II, where only benthic foraminifera exhibit negative $\delta^{13}\text{C}$ values. In this scenario, methane activity is sufficiently high as to surpass the SMTZ and oxidized less efficiently with the consequence of lower AOM rates and higher methane fluxes into the bottom waters. The methane escaped is then partially oxidized by methanotrophic aerobic microbes in the water column. In this scenario the negative $\delta^{13}\text{C}$ values are likely to be the result of calcification in the presence of ^{13}C -depleted DIC and probably ingestion of ^{13}C -depleted methanotrophic microbes on which foraminifera feed. (b) Schematic diagram showing how methane flux controls the SMTZ if the flux of sulfate (SO_4^{2-}) from the seawater and the characteristics of the sediments are constant. Arrow size is proportional to upward methane flux. Modified after Borowski et al. (1996). (c) Schematic diagram representing CIE I, where both benthic and planktonic foraminifera exhibit negative $\delta^{13}\text{C}$ values. In this case the methane flux is low and upward fluxes of methane and downward fluxes of sulfate (coming from the sea water) meet within the SMTZ and the anaerobic oxidation of methane (AOM) can take place (e.g. Boetius et al., 2000; Knittel and Boetius, 2009). Here, sulfate and methane may be consumed simultaneously according to Eq. (1). The production of bicarbonate from AOM can induce the precipitation of calcium carbonate, so-called methane-derived authigenic carbonates, on the benthic and planktonic foraminifera tests after burial through Eq. (2).

According to Borowski et al. (1996) methane-derived authigenic carbonate precipitation occur when the methane flux is low and all the methane is oxidized by AOM within the SMTZ. It is also possible that the primary test of the benthic foraminifera was already depleted in ^{13}C (orange benthic foraminifera in Fig. 9c), and the negative values of the secondary carbonate overgrowth were cumulatively added (see above).

These observations give rise to several questions and hypotheses about the possibility by benthic foraminifera to record past methane emissions. Further measurements on foraminifera from methane seep sites and experiments are necessary to better understand how methane emissions from different sources can affect the foraminiferal shells and the sort of information that can be obtained from analysis of the isotope composition of their tests.

5.3 North Atlantic deglacial CIEs

Similar negative excursions in foraminiferal ^{13}C records have been reported in several Quaternary isotope records and

have been interpreted as evidence for methane release (Kennett et al., 2000; Smith et al., 2001; Keigwin, 2002; Millo et al., 2005b; Cook et al., 2011; Hill et al., 2012). In particular, low $\delta^{13}\text{C}$ values during the deglaciation have also been reported by Smith et al. (2001) in stable isotope records from the East Greenland continental shelf (cores JM96 in Fig. 1). In order to compare these events with the Vestnesa Ridge record (Fig. 10), the original radiocarbon ages of Smith et al. (2001) have been re-calibrated with Calib 7.0 (see above). No regional correction has been applied for the deeper cores (JM96-1214: 574 mwd; JM96-1215: 668 mwd) as suggested by Jennings et al. (2006), whereas in the shallow core (JM96-1207: 404 mwd) a correction of $\Delta R = -150$ years has been applied, following Jennings et al. (2002). The first (14.4–14.2 ka; -3.5‰ for *C. neoteretis*) and second (12.9 ka; -4.8‰ for *N. pachyderma* (s)) isotopic excursions in the East Greenland record are close in time to the beginning and the end of CIE I, respectively (Fig. 10b). The third excursion (10.9–9.7 ka; -6.4‰ for *N. pachyderma* s, -3.8‰ for *Cibicides lobatulus*) is coeval with CIE II but lasted longer (Fig. 10b).

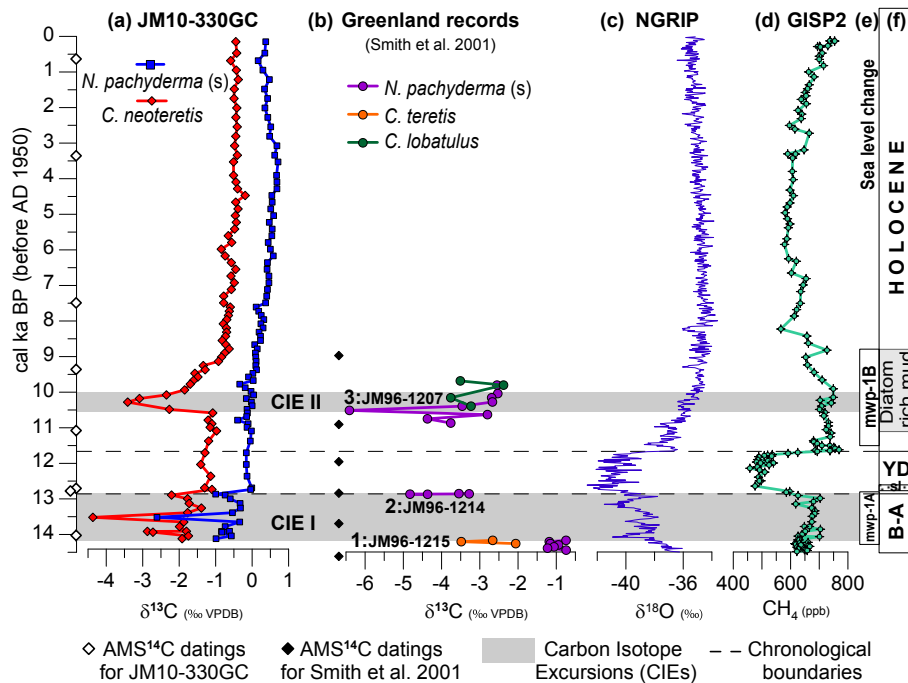


Figure 10. Isotopic data of core JM10-330GC and other records plotted versus cal ka BP (before AD 1950): (a) $\delta^{13}\text{C}$ record of *N. pachyderma* (s) (blue line) and of *C. neoteretis* (red line) from JM10-330GC; (b) $\delta^{13}\text{C}$ negative excursions from east Greenland continental shelf (Smith et al., 2001): event 1 from core JM96-1215, event 2 from core JM96-1214, and event 3 from core JM96-1207; (c) NorthGRIP ice core $\delta^{18}\text{O}$ record (Andersen et al., 2004); (d) Greenland Ice Sheet Project 2 (GISP2) atmospheric CH_4 record (Brook et al., 2000); (e) melt water pulse mwp-1A and mwp-1B (Peltier and Fairbanks, 2006; Stanford et al., 2011); (f) stratigraphy obtained for JM10-330GC with chronological subdivisions (dashed lines). White diamonds on the y axis indicate dating points for JM10-330GC (next to plot a) and black diamonds next to plot (b) are dating points for cores of Smith et al. (2001). Shaded horizontal bars indicate carbon isotope excursions CIE I and CIE II. Abbreviations: B-A, Bølling–Allerød; YD, Younger Dryas; sl, sandy layer.

Negative $\delta^{13}\text{C}$ excursions during glacial and deglacial times in the Nyegga pockmark field (800–1000 mwd, NPF in Fig. 1) have been recently reported (Hill et al., 2012). The seepage in this area was particularly active between 15 and 13 ka, with several $\delta^{13}\text{C}$ negative excursions (as low as -6‰) in both benthonic and planktonic records, while around 9 ka a negative $\delta^{13}\text{C}$ excursion is present in the benthonic record (-2.7‰), but not reflected in the planktonic record (Hill et al., 2012).

The similarity in timing of these carbon isotope excursions over long distances and wide water depth ranges (Fig. 1) is remarkable and suggests that the CIEs could be regional at the scale of the North Atlantic Ocean to the Fram Strait.

Both the Bølling–Allerød interstadials and the early Holocene are periods of climate warming during the deglaciation (Andersen et al., 2004) (Fig. 10c) and are characterized by increased CH_4 concentration in the atmosphere (Brook et al., 2000; GISP2) (Fig. 10d). They also occur during periods of rapid sea-level rise (melt water pulse mwp-1A: 14.3–12.8 ka; mwp-1B: 11.5–8.8 ka; Fig. 10e) (Peltier and Fairbanks, 2006; Stanford et al., 2011). These findings suggest an apparent correlation between methane events in

the North Atlantic and the Fram Strait and climatic events at global or regional scale.

Since the methane that escapes from the seafloor is rapidly oxidized in the water column, we do not expect a short-term change in stable carbon isotope composition of the North Atlantic deep water. The foraminiferal records published so far (e.g. Volkman and Mensch, 2001; Wollenburg et al., 2001; Nørgaard-Pedersen et al., 2003; Sarnthein et al., 2003; Aagaard-Sørensen et al., 2010; Jessen et al., 2010) confirm this interpretation. However, the presence of local carbon isotope perturbation at the same time in multiple locations (Fig. 1) is remarkable, and possible common triggering mechanisms need to be considered.

We are currently working on several cores from the Vestnesa Ridge in order to understand whether the negative carbon anomalies recorded by foraminifera are due to local or global processes and whether the apparent correlation with climatic events can be proved.

5.4 Possible triggering mechanisms and connection with climate change?

It is still not possible to determine whether present-day gas emissions on the eastern part of the Vestnesa Ridge are sourced from below the GHSZ (gas hydrate stability zone), directly from dissociation of gas hydrates, or from a combination of deeper and shallower processes (Bünz et al., 2012; Smith et al., 2014). It is also unclear whether focused fluid flow pathways from the base of the GHSZ have been established recently at the end of the last glaciation, or whether they have existed for much longer and have been reactivated multiple times. Even though this study has only documented two former events of increased emission at the western end of the Vestnesa Ridge, it favours a model of reactivation of chimney structures. The gas emissions and reactivation seem to occur during periods of climate change similar to observations from the mid-Norwegian margin, where the generation and initiation of focused fluid flow is most likely related to an overpressure due to a combined effect of loading of glaciogenic sediments and shelf ice glaciation (Hustoft et al., 2009b; Plaza-Faverola et al., 2011). However, the initial generation of such chimney structures and their reactivation might each be related to different geological processes. Chimneys are usually conceived as a network of connected small-scale fractures originating from natural hydraulic fracturing (Arntsen et al., 2007). They represent pre-existing zones of weakness and open pathways that might facilitate fluid flow much more easily than during the initial generation of the fracture network. In deep-water areas these fractures might be filled with gas hydrate (Kim et al., 2011).

The apparent climate forcing of gas emission in the western part of the Vestnesa Ridge documented herein could be the result of the individual or combined effect of sea-level rise, increased seismicity, elevated sedimentation rates and/or gas hydrate dissociation. From the above-mentioned processes it seems unlikely that gas hydrate dissociation and loading of glaciogenic sediment have played a major role given that our study area is in deep water, far away from the shelf edge, and that the timing of the deposition of large amount of glaciogenic sediments (Ottesen et al., 2005; Mattingdal et al., 2014) does not coincide with the venting periods documented herein.

Both CIEs occur at times when deep convection and generation of cold bottom water is strong (McManus et al., 2004; Ezat et al., 2014). The high $\delta^{18}\text{O}_{\text{ICV}}$ values of the benthonic record during CIE I confirm that the area was bathed in cold water during the B-A interval (Fig. 4d). During CIE II, the marked shift in the planktonic assemblage (previously dominated by the polar species *N. pachyderma* (s) and subsequently by the subpolar species *T. quinqueloba*; Fig. 4a) indicates a surface water warming. The presence of two relatively light excursions of benthonic $\delta^{18}\text{O}_{\text{ICV}}$ ($< 0.7\text{‰}$; Fig. 4d) indicates a small warming of the bottom water (see Rasmussen et al., 2007, 2014; Ezat et al., 2014; Groot et al., 2014), but

this warming is certainly too small to start gas hydrate dissociation. Hydrate dissociation at such a depth would require a substantial warming before any gas could escape from deeper buried sediments ($> 1000\text{ mwd}$) (Reagan and Moridis, 2007), although hydrates buried at shallower depth within chimneys could be affected to some extent and release gas at the seabed (Smith et al., 2014).

The present sedimentation rate on the Vestnesa Ridge is about 19 cm ka^{-1} , whereas it was considerably higher ($40\text{--}50\text{ cm ka}^{-1}$; Fig. 3 and Table 1) during the deglaciation. Around 14.6 to 14.3 ka, sedimentation rates on the western Svalbard margin increased over large areas to $> 5\text{ m ka}^{-1}$ (Jessen et al., 2010 and references therein). However, it is not known whether such a relatively small loading alone could have significantly increased fluid overpressure in the subsurface resulting in methane release at the seabed.

Sea level, on the other hand, has risen considerably after the last glaciation, and the two documented CIEs correlate well with two major melt water pulses (mwp-1A and mwp-1B; Peltier and Fairbanks, 2006; Stanford et al., 2011) (Fig. 10e). Global sea-level rise has been implicated in triggering of landslides by causing an increase in excess pore pressure in the sub-seafloor during the deglaciation and the Holocene in the northern North Atlantic sector (Owen et al., 2007; McGuire and Maslin, 2012). However, the hydrostatic pressure increase would only affect excess pore pressures if impermeable sediments or a complex subsurface structure traps the pores. These trapping mechanisms might be provided by gas hydrates that clog the pore space along the BSR or fill the fractures of gas chimneys (Nimblett et al., 2003; Kim et al., 2011). A cumulative effect of sedimentation and sea-level rise has potentially elevated excess pore pressure to initiate gas migration along the fracture network within a chimney.

Moreover, sea-level rise, elevated sedimentation rates in the whole study area, and the isostatic rebound following the retreat of the glaciers (Landvik et al., 1998; Forman et al., 2004; Bungum et al., 2005) may foster other processes, such as lithospheric stress changes, resulting in increased seismicity. Modelling studies (Wallmann et al., 1988; Nakada et al., 1992) have demonstrated that sea-level changes are capable of triggering or modulating tectonic activity. More specifically, Luttrell and Sandwell (2010) showed that lithospheric flexure due to ocean loading caused by post-glacial sea-level rise was sufficient to promote failure through the reduction of normal stress, thereby reactivating faults.

Increased seismicity might have had a two-fold effect on the fluid flow system in the Vestnesa Ridge. It might have led to an increased supply of gas along deep-seated faults, leading to an increase in pore pressures beneath the hydrate-bearing sediments. Furthermore, it might have led to an excitation and dilation of fractures within the chimney structures, leading to the leakage of gas, similar to what has been observed on the Bear Island Fan (Franek et al., 2014).

We cannot conclusively distinguish which factors triggered gas venting in the two periods at the end of and shortly after the last glaciation, but we suggest that a combined effect of sea-level rise, sedimentation and seismicity might have led to increased pore pressures in an already overpressured system, thereby promoting and initiating gas venting from the seabed at the western part of the Vestnesa Ridge.

6 Conclusions

We have presented new data from a sediment core collected at the Vestnesa Ridge in the eastern part of the Fram Strait, the deep-water gateway to the Arctic Ocean. Here, a sediment core was retrieved from an apparently inactive pockmark in the western, deeper part of the Vestnesa Ridge. The results show a surprisingly undisturbed sedimentary record that allows for establishment of a detailed methane release event chronology for the last 14 kyr. The benthonic $\delta^{13}\text{C}$ record shows negative carbon isotope excursions (CIEs) as low as -4.37‰ during the Bølling–Allerød interstadials (CIE I) and as low as -3.41‰ in the early Holocene (CIE II). The persistence of negative values (as low as -2.75‰) after a thorough cleaning procedure, which was designed to remove all authigenic carbonate coatings on benthonic foraminiferal tests from CIE I samples, indicates that ^{13}C -depleted values of diagenetic overgrowth of shells of *C. neoteretis* are cumulatively added to the already negative values of the primary test.

The planktonic foraminifera $\delta^{13}\text{C}$ record shows a similar negative trend during the CIE I (with values as low as -2.61‰), but during CIE II the values are within the normal marine range (-0.5‰ to 1‰). SEM investigations confirm the presence of a thin AOM-derived coating on the *N. pachyderma* tests exclusively from the CIE I interval.

During CIE I in the Bølling–Allerød, the negative ^{13}C values in both benthonic and planktonic foraminifera have been interpreted as being due to methane-derived authigenic carbonates. During CIE II in the early Holocene, only benthonic foraminifera exhibit negative ^{13}C values, which in this case have been interpreted as the result of the incorporation of ^{13}C -depleted carbon from methane emissions during the primary biomineralization of the tests and probably ingestion of ^{13}C -depleted methanotrophic microbes on which foraminifera feed. It is also possible that early authigenic carbonates, such as AOM products in surface sediments, were precipitated on the benthonic foraminiferal tests when they were still alive.

Methane release events with similar timing have been reported in several locations in the North Atlantic and, together with our new observation, point to a more regional event, showing an apparent correlation with northern climatic events.

We suggest that a combined effect of sea-level rise, high sediment loading and increased seismicity during the

deglaciation could have led to increased pore pressures, therefore promoting and initiating gas venting from the seafloor in the Vestnesa Ridge, eastern Fram Strait. The methane contribution from the ocean floor to the water column and the atmosphere remains to be quantified.

The Supplement related to this article is available online at doi:10.5194/cp-11-669-2015-supplement.

Acknowledgements. This research is part of the Centre for Arctic Gas Hydrate, Environment and Climate (CAGE) funded by the Norwegian Research Council (grant no. 223259). Additional funding came from the European project HERMIONE of the 7th Framework Programme environment including climate change (grant no. 226354), from the PNRA project FORMAT and from the Paleo-CIRCUS project supported by the Mohn Foundation and UiT Arctic University of Tromsø. We are grateful to the captain, crew and scientific party on board R/V *Helmer Hanssen* for help in collecting the core. We thank the staff at the Electron Microscopy Centre at Plymouth University (UK) for assistance during SEM and EDS analysis. We acknowledge the assistance of J. P. Holm with Fig. 1 and Torger Grytå with Fig. 9. Great improvements were made to the manuscript thanks to the constructive reviews by G. Dickens and L. J. de Nooijer. M. B. Hart is thanked for the friendly review of the revised manuscript.

Edited by: A. Sluijs

References

- Aagaard, K., Swift, J. H., and Carmack, E. C.: Thermohaline circulation in the Arctic Mediterranean Seas, *J. Geophys. Res.*, 90, 4833–4846, 1985.
- Aagaard, K., Foldvik, A., and Hillman, S. R.: The West Spitsbergen Current: disposition and water mass transformation, *J. Geophys. Res.*, 92, 3778–3784, 1987.
- Aagaard-Sørensen, S., Husum, K., Hald, M., and Knies, J.: Paleoceanographic development in the SW Barents Sea during the Late Weichselian–Early Holocene transition, *Quaternary Sci. Rev.*, 29, 3442–3456, 2010.
- Andersen, K. K., Azuma, N., Barnola, J.-M., Bigler, M., Biscaye, P., Caillon, N., Chappellaz, J., Clausen, H. B., Dahl-Jensen, D., Fischer, H., Flückiger, J., Fritzsche, D., Fujii, Y., Goto-Azuma, K., Grønbold, K., Gundestrup, N. S., Hansson, M., Huber, C., Hvidberg, C. S., Johnsen, S. J., Jonsell, U., Jouzel, J., Kipfstuhl, S., Landais, A., Leuenberger, M., Lorrain, R., Masson-Delmotte, V., Miller, H., Motoyama, H., Narita, H., Popp, T., Rasmussen, S. O., Raynaud, D., Rothlisberger, R., Ruth, U., Samyn, D., Schwander, J., Shoji, H., Siggard-Andersen, M.-L., Steffensen, J. P., Stocker, T., Sveinbrönsdóttir, A. E., Svensson, A., Takata, M., Tison, J.-L., Thorsteinsson, Th., Watanabe, O., Wilhelms, F., and White, J. W. C.: High-resolution record of Northern Hemisphere climate extending into the last interglacial period, *Nature*, 431, 147–151, 2004.

- Arntsen, B., Wensaas, L., Loseth, H., and Hermanrud, C.: Seismic modeling of gas chimneys, *Geophysics*, 72, 251–259, 2007.
- Austin, W. E. N., Telford, R. J., Ninnemann, U. S., Brown, L., Wilson, L. J., Small, D. P., and Bryant, C. L.: North Atlantic reservoir ages linked to high Younger Dryas atmospheric radiocarbon concentrations, *Global Planet. Change*, 79, 226–233, 2011.
- Bard, E., Arnold, M., Mangerud, J., Paterne, M., Labeyrie, L., Duprat, J., Mélières, M.-A., Sønstegeard, E., and Duplessy, J.-C.: The North Atlantic atmosphere-sea surface ^{14}C gradient during the Younger Dryas climatic event, *Earth Planet. Sci. Lett.*, 126, 275–287, 1994.
- Barnes, R. O. and Goldberg, E. D.: Methane production and consumption in anoxic marine sediments, *Geology*, 4, 297–300, 1976.
- Berndt, C., Feseker, T., Treude, T., Krastel, S., Liebetrau, V., Niemann, H., Bertics, V. J., Dumke, I., Dünnebier, K., Ferré, B., Graves, C., Gross, F., Hissmann, K., Hühnerbach, V., Krause, S., Lieser, K., Schauer, J., and Steinle, L.: Temporal constraints on hydrate-controlled methane seepage off Svalbard, *Science*, 343, 284–287, 2014.
- Biastoch, A., Treude, T., Rüpke, L. H., Riebesell, U., Roth, C., Burwicz, E. B., Park, W., Latif, M., Böning, C. W., Madec, G., and Wallmann, K.: Rising Arctic Ocean temperatures cause gas hydrate destabilization and ocean acidification, *Geophys. Res. Lett.*, 38, L08602, doi:10.1029/2011GL047222, 2011.
- Boettius, A. and Wenzhöfer, F.: Seafloor oxygen consumption fuelled by methane from cold seeps, *Nat. Geosci.*, 6, 725–734, doi:10.1038/ngeo1926, 2013.
- Boetius, A., Ravensschlag, K., Schubert, C. J., Rickert, D., Widel, F., Gieseke, A., Amann, R., Jørgensen, B. B., Witte, U., and Pfannkuche, O.: A marine microbial consortium apparently mediating anaerobic oxidation of methane, *Nature*, 407, 623–626, 2000.
- Bohrmann, G., Greinert, J., Suess, E., and Torres, M.: Authigenic carbonates from the Cascadia subduction zone and their relation to gas hydrate stability, *Geology*, 26, 647–650, 1998.
- Bondevik, S., Mangerud, J., Birks, H. H., Gulliksen, S., and Reimer, P.: Changes in North Atlantic radiocarbon reservoir ages during the Allerød and Younger Dryas, *Science*, 312, 1514–1517, 2006.
- Borowski, W., Paull, C. K., and Ussler III, W.: Marine pore-water sulphate profiles indicate in situ methane flux from underlying gas hydrate, *Geology*, 24, 655–658, 1996.
- Boyle, E. A. and Rosenthal, Y.: Chemical hydrography of the South Atlantic during the Last Glacial Maximum: $\delta^{13}\text{C}$ vs. Cd, in: *The South Atlantic: Present and Past Circulation*, edited by: Wefer, G., Berger, W. H., Siedler, G., and Webb, D. J., Springer Verlag, New York, 423–443, ISBN: 978-3-642-80353-6, 1996.
- Brook, E. J., Harder, S., Severinghaus, J., Steig, E. J., and Sucher, C. M.: On the origin and timing of rapid changes in atmospheric methane during the last glacial period, *Global Biogeochem. Cy.*, 14, 559–572, 2000.
- Bungum, H., Lindholm, C., and Faleide, J. I.: Postglacial seismicity offshore mid-Norway with emphasis on spatio-temporal-magnitudinal variations, *Mar. Petrol. Geol.*, 22, 137–148, 2005.
- Bünz, S., Polyanov, S., Vadakkepuliambatta, S., Consolaro, C., and Mienert, J.: Active gas venting through hydrate-bearing sediments on the Vestnesa Ridge, offshore W-Svalbard, *Mar. Geol.*, 332–334, 189–197, 2012.
- Castellini, D. G., Dickens, G. R., Snyder, G. T., and Ruppel, C. D.: Barium cycling in shallow sediment above active mud volcanoes in the Gulf of Mexico, *Chem. Geol.*, 226, 1–30, 2006.
- Cook, M. S., Keigwin, L. D., Birgel, D., and Hinrichs, K.-U.: Repeated pulses of vertical methane flux recorded in glacial sediments from the southeast Bering Sea, *Paleoceanography*, 26, PA2210, doi:10.1029/2010PA001993, 2011.
- Dickens, G.: On the fate of past gas: What happens to methane released from a bacterially mediated gas hydrate capacitor?, *Geochem. Geophys. Geosy.*, 2, 2000GC000131, doi:10.1029/2000GC000131, 2001.
- Ezat, M., Rasmussen, T. L., and Groenewald, J.: Persistent intermediate water warming during cold stadials in the southeastern Nordic seas during the past 65 k.y., *Geology*, 42, 663–666, doi:10.1130/G35579.1, 2014.
- Engen, Ø., Faleide, J. I., and Dyreng, T. K.: Opening of the Fram Strait gateway: A review of plate tectonic constraints, *Tectonophysics*, 450, 51–69, 2008.
- Fairbanks, R. G.: A 17 000-year glacio-eustatic sea level record: influence of glacial melting rates on the Younger Dryas event and deep-ocean circulation, *Nature*, 342, 637–742, 1989.
- Ferré, B., Mienert, J., and Feseker, T.: Ocean temperature variability for the past 60 years in the Norwegian-Svalbard margin influences gas hydrate stability on human time scale, *J. Geophys. Res.*, 117, C10017, doi:10.1029/2012JC008300, 2012.
- Forman, S. L., Lubinski, D. J., Ingólfsson, Ó., Zeeberg, J. J., Snyder, J. A., Siegert, M. J., and Matishov, G. G.: A review of postglacial emergence on Svalbard, Franz Josef Land and Novaya Zemlya, northern Eurasia, *Quaternary Sci. Rev.*, 23, 1391–1434, 2004.
- Franek, P., Mienert, J., Bünz, S., and Géli, L.: Character of seismic motion at a location of a gas hydrate-bearing mud volcano on the SW Barents Sea margin, *J. Geophys. Res.-Sol. Ea.*, 119, 2014JB010990, doi:10.1002/2014JB010990, 2014.
- Greinert, J., Bohrmann, G., and Suess, E.: Gas hydrate-associated carbonates and methane-venting at Hydrate Ridge: classification, distribution, and origin of authigenic lithologies, in: *Natural Gas Hydrates: Occurrence, Distribution, and Detection*, edited by: Paull, C. K. and Dillon, W. P., AGU Geoph. Monog., 124, American Geophysical Union, Washington, DC, 99–113, 2001.
- Groot, D. E., Aagaard-Sørensen, S., and Husum, K.: Reconstruction of Atlantic water variability during the Holocene in the western Barents Sea, *Clim. Past*, 10, 51–62, doi:10.5194/cp-10-51-2014, 2014.
- Hill, T. M., Kennett, J. P., and Spero, H. J.: Foraminifera as indicators of methane-rich environments: a study of modern methane seeps in Santa Barbara channel, California, *Mar. Micropaleontol.*, 49, 123–138, 2003.
- Hill, T. M., Kennett, J. P., and Valentine, D. L.: Isotopic evidence for the incorporation of methane-derived carbon into foraminifera from modern methane seeps, Hydrate Ridge, Northeast Pacific, *Geochim. Cosmochim. Ac.*, 68, 4619–4627, 2004.
- Hill, T. M., Paull, C. K., and Crister, R. B.: Glacial and deglacial seafloor methane emissions from pockmarks on the northern flank of the Storegga Slide complex, *Geo-Mar. Lett.*, 32, 73–84, 2012.
- Hinrichs, K.-U. and Boetius, A.: The anaerobic oxidation of methane: New insights in microbial ecology and biogeochemistry, in: *Ocean Margin Systems*, edited by: Wefer, G., Billett, D.,

- and Hebbeln, D., Springer Verlag, Berlin, Heidelberg, 457–477, 2002.
- Hustoft, S., Bunz, S., Mienert, J., and Chand, S.: Gas hydrate reservoir and active methane-venting province in sediments on <20 Ma young oceanic crust in the Fram Strait, offshore NW-Svalbard, *Earth Planet. Sc. Lett.*, 284, 12–24, 2009a.
- Hustoft, S., Dugan, B., and Mienert, J.: Effects of rapid sedimentation on developing the Nyegga pockmark field: Constraints from hydrological modeling and 3-D seismic data, offshore mid-Norway, *Geochem. Geophys. Geosy.*, 10, Q06012, doi:10.1029/2009GC002409, 2009b.
- Iversen, N. and Jørgensen, B. B.: Anaerobic methane oxidation rates at the sulfate-methane transition in marine sediments from Kattegat and Skagerrak (Denmark), *Limnol. Oceanogr.*, 30, 944–955, 1985.
- Jennings, A. E., Knudsen, K. L., Hald, M., Carsten, V. H., and Andrews, J. T.: A mid-Holocene shift in Arctic sea-ice variability on the East Greenland Shelf, *The Holocene*, 12, 49–58, 2002.
- Jennings, A. E., Hald, M., Smith, M., and Andrews, J. T.: Freshwater forcing from the Greenland Ice Sheet during the Younger Dryas: evidence from southeastern Greenland shelf cores, *Quaternary Sci. Rev.*, 25, 282–298, 2006.
- Jessen, S. P., Rasmussen, T. L., Nielsen, T., and Solheim, A.: A new Late Weichselian and Holocene marine chronology for the western Svalbard slope 30 000–0 cal years, *Quaternary Sci. Rev.*, 29, 1301–1312, 2010.
- Judd, A. G. and Hovland, M.: *Seabed Fluid Flow: the Impact on Geology, Biology, and the Marine Environment*, Cambridge University Press, 475 pp., 2007.
- Keigwin, L. D.: Late Pleistocene–Holocene paleoceanography and ventilation of the Gulf of California, *J. Oceanogr.*, 58, 421–432, 2002.
- Kennett, J. P., Cannariato, K. G., Hendy, I. L., and Behl, R. J.: Carbon Isotopic evidence for methane hydrate instability during Quaternary interstadials, *Science*, 288, 128–133, 2000.
- Kim, G. Y., Yi, B. Y., Yoo, D. G., Ryu, B. J., and Riedel, M.: Evidence of gas hydrate from downhole logging data in the Ulleung Basin, East Sea, *Mar. Petrol. Geol.*, 28, 1979–1985, 2011.
- Knittel, K. and Boetius, A.: Anaerobic oxidation of methane: progress with an unknown process, *Annu. Rev. Microbiol.*, 63, 311–334, 2009.
- Kuechler, R. R., Birgel, D., Kiel, S., Freiwald, A., Goedert, J. I., Thiel, V., and Peckmann, J.: Miocene methane-derived carbonates from southwestern Washington, USA and a model for silicification at seeps, *Lethaia*, 45, 259–273, 2012.
- Kulm, L. D. and Suess, E.: Relationship between carbonate deposits and fluid venting: Oregon accretionary prism, *J. Geophys. Res.*, 95, 8899–8915, 1990.
- Landvik, J. Y., Bondevik, S., Elverhøi, A., Fjeldskaar, W., Mangerud, J., Salvigsen, O., Siegert, M. J., Svendsen, J.-I., and Vorren, T. O.: The last Glacial Maximum of Svalbard and the Barents Sea area: ice sheet extent and configuration, *Quaternary Sci. Rev.*, 17, 43–75, 1998.
- Lubinski, D. J., Polyak, L., and Forman, S. L.: Freshwater and Atlantic water inflows to deep northern Barents and Kara seas since ca 13 14C ka: foraminifera and stable isotopes, *Quaternary Sci. Rev.*, 20, 1851–1879, 2001.
- Luttrell, K. and Sandwell, D.: Ocean loading effects on stress at near shore plate boundary fault systems, *J. Geophys. Res.-Sol. Ea.*, 115, B08411, 2010.
- Mackensen, A., Wollenburg, J., and Licari, L.: Low $\delta^{13}\text{C}$ in tests of live epibenthonic and endobenthonic foraminifera at a site of active methane seepage, *Paleoceanography*, 12, PA2022, doi:10.1029/2005PA001196, 2006.
- Mangerud, J. and Gulliksen, S.: Apparent radiocarbon ages of recent marine shells from Norway, Spitsbergen, and Arctic Canada, *Quaternary Res.*, 5, 263–273, 1975.
- Mangerud, J., Bondevik, S., Gulliksen, S., Hufthammer, A. K., and Høisæter, T.: Marine ^{14}C reservoir ages for 19th century whales and molluscs from the North Atlantic, *Quaternary Sci. Rev.*, 25, 3228–3245, 2006.
- Martin, R. A., Shelley, A. D., Rathburn, A. E., and Perez, M. E.: Relationships between the stable isotopic signatures of living and fossil foraminifera in Monterey Bay, California, *Geochem. Geophys. Geosy.*, 5, Q04004, doi:10.1029/2003GC000629, 2004.
- Martin, R. A., Nesbitt, E. A., and Campbell, K. A.: Carbon stable isotopic composition of benthic foraminifera from Pliocene cold methane seeps, Cascadia accretionary margin, *Palaeogeogr. Palaeoclimatol. Palaeoecol.*, 246, 260–277, 2007.
- Martin, R. A., Nesbitt, E. A., and Campbell, K. A.: The effect of anaerobic methane oxidation on benthic foraminiferal assemblages and stable isotopes on the Hikurangi Margin of eastern New Zealand, *Mar. Geol.*, 272, 270–284, 2010.
- Mattingsdal, R., Knies, J., Andreassen, K., Fabian, K., Husum, K., Grøsfjeld, K., and De Schepper, S.: A new 6 Myr stratigraphic framework for the Atlantic–Arctic Gateway, *Quaternary Sci. Rev.*, 92, 170–178, 2014.
- McGuire, B. and Maslin, M.: *Climate Forcing of Geological Hazards*, John Wiley-Blackwell, West Sussex, UK, 3268 pp., ISBN: 978-0-470-65865-9, 2012.
- McManus, J. F., Francois, R., Gherardi, J.-M., Keigwin, L. D., and Brown-Ledger, S.: Collapse and rapid resumption of Atlantic meridional circulation linked to deglacial climate changes, *Nature*, 428, 834–837, 2004.
- Millo, C., Sarnthein, M., Erlenkeuser, H., Grootes, P. M., and Andersen, N.: Methane-induced early diagenesis of foraminiferal tests in the southwestern Greenland Sea, *Mar. Micropaleontol.*, 58, 1–12, 2005a.
- Millo, C., Sarnthein, M., Erlenkeuser, H., and Frederichs, T.: Methane-driven late Pleistocene $\delta^{13}\text{C}$ minima and overflow reversals in the southwestern Greenland Sea, *Geology*, 33, 873–876, 2005b.
- Nakada, M. and Yokose, H.: Ice age as a trigger of active Quaternary volcanism and tectonism, *Tectonophysics*, 212, 321–329, 1992.
- Niemann, H., Lösekann, T., de Beer, D., Elvert, M., Nadalig, T., Knittel, K., Amann, R., Sauter, E. J., Schlüter, M., Klages, M., Foucher, J. P., and Boetius, A.: Novel microbial communities of the Haakon Mosby mud volcano and their role as a methane sink, *Nature*, 443, 854–858, 2006.
- Niewöhner, C., Hensen, C., Kasten, S., Zabel, M., and Schulz, H. D.: Deep sulfate reduction completely mediated by anaerobic methane oxidation in sediments of the upwelling area off Namibia, *Geochim. Cosmochim. Ac.*, 62, 455–464, 1998.
- Nimblett, J. and Ruppel, C.: Permeability evolution during the formation of gas hydrates in marine sediments, *J. Geophys. Res.-Sol. Ea.*, 108, B9, 2420, doi:10.1029/2001JB001650, 2003.

- Nørgaard-Pedersen, N., Spielhagen, R.-F., Erlenkeuser, H., Grootes, P. M., Heinemeier, J., and Knies, J.: Arctic Ocean during the Last Glacial Maximum: Atlantic water and polar domains of surface water mass distribution and ice cover, *Paleoceanography*, 18, 1063, doi:10.1029/2002PA000781, 2003.
- Ottesen, D., Dowdeswell, J. A., and Rise, L.: Submarine landforms and the reconstruction of fast-flowing ice streams within a large Quaternary ice sheet: the 2500-km-long Norwegian-Svalbard margin (57°–80° N), *Geol. Soc. Am. Bull.*, 117, 1033–1050, 2005.
- Owen, M., Day, S., and Maslin, M.: Late Pleistocene submarine mass movements: occurrence and causes, *Quaternary Sci. Rev.*, 26, 958–978, 2007.
- Panieri, G., Camerlenghi, A., Conti, S., Pini, G. A., and Cacho, I.: Methane seepages recorded in benthonic foraminifera from Miocene seep carbonates, Northern Apennines (Italy), *Palaeogeogr. Palaeoclimatol. Palaeoecol.*, 284, 271–282, 2009.
- Panieri, G., Camerlenghi, A., Cacho, I., Carvera, C. S., Canals, M., Lafuerza, S., and Herrera, G.: Tracing seafloor methane emissions with benthonic foraminifera: Results from the Ana submarine landslide (Eivissa Channel, Western Mediterranean Sea), *Mar. Geol.*, 291–294, 97–112, doi:10.1016/j.margeo.2011.11.005, 2012.
- Panieri, G., Aharun, P., Sen Gupta, B. K., Camerlenghi, A., Palmer Ferrer, F., and Cacho, I.: Late Holocene foraminifera of Blake Ridge diapir: Assemblage variation and stable-isotope record in gas-hydrate bearing sediments, *Mar. Geol.*, 353, 99–107, 2014a.
- Panieri, G., James, R. H., Camerlenghi, A., Westbrooks, G. K., Consolaro, C., Cacho, I., Cesari, V., and Cervera, C. S.: Record of methane emission from the West Svalbard continental margin during the last 23.5 ka revealed by $\delta^{13}\text{C}$ of benthonic foraminifera, *Global Planet. Change*, 122, 151–160, 2014b.
- Paull, C. K., Ussler III, W., Lorenson, T., Winters, W., and Dougherty, J.: Geochemical constraints on the distribution of gas hydrates in the Gulf of Mexico, *Geo-Mar. Lett.*, 25, 273–280, 2005.
- Peckmann, J., Reimer, A., Luth, U., Luth, C., Hansen, B. T., Heinicke, C., Hoefs, J., and Reitner, J.: Methane-derived carbonates and authigenic pyrite from the northwestern Black Sea, *Mar. Geol.*, 177, 129–150, 2001.
- Peltier, W. R. and Fairbanks, R. G.: Global glacial ice volume and Last Glacial Maximum duration from an extended Barbados sea level record, *Quaternary Sci. Rev.*, 25, 3322–3337, 2006.
- Pena, L. D., Calvo, E., Cacho, I., Eggins, S., and Palejero, C.: Identification and removal of Mn-Mg-rich contaminant phases in foraminiferal tests: Implications for Mg/Ca past temperature reconstructions, *Geochem. Geophys. Geosy.*, 6, Q09P02, doi:10.1029/2005GC000930, 2005.
- Pena, L. D., Cacho, I., Calvo, E., Palejero, C., Eggins, S., and Sadekov, A.: Characterization of contaminant phases in foraminifera carbonates by electron microprobe mapping, *Geochem. Geophys. Geosy.*, 9, Q07012, doi:10.1029/2008GC002018, 2008.
- Petersen, C. J., Bünz, S., Hustoft, S., Mienert, J., and Klaeschen, D.: High-resolution P-Cable 3D seismic imaging of gas chimney structures in gas hydrated sediments of an Arctic sediment drift, *Mar. Petrol. Geol.*, 27, 1981–1994, 2010.
- Plaza-Faverola, A., Bünz, S., and Mienert, J.: Repeated fluid expulsion through sub-seabed chimneys offshore Norway in response to glacial cycles, *Earth Planet. Sc. Lett.*, 305, 297–308, 2011.
- Rasmussen, S. O., Andersen, K. K., Svensson, A. M., Steffensen, J. P., Vinther, B. M., Clausen, H. B., Siggaard-Andersen, M.-L., Johnsen, S. J., Larsen, L. B., Dahl-Jensen, D., Bigler, M., Röthlisberger, R., Fischer, H., Goto-Azuma, K., Hansson, M. E., and Ruth, U.: A new Greenland ice core chronology for the last glacial termination, *J. Geophys. Res.*, 111, D06102, doi:10.1029/2005JD006079, 2006.
- Rasmussen, T. L., Thomsen, E., Ślubowska, M. A., Jessen, S. P., Solheim, A., and Koç, N.: Paleoceanographic evolution of the SW Svalbard margin (76° N) since 20 000 ^{14}C yr BP, *Quaternary Res.*, 67, 100–114, 2007.
- Rasmussen, T. L., Thomsen, E., and Nielsen, T.: Water mass exchange between the Nordic seas and the Arctic Ocean on millennial time scale during MIS 4–MIS 2, *Geochem. Geophys. Geosy.*, 15, 53–544, doi:10.1002/2013GC005020, 2014.
- Rathburn, A. E., Pérez, M. E., Martin, J. B., Day, S. A., Mahn, C., Gieskes, J., Ziebis, W., Williams, D., and Bahls, A.: Relationships between the distribution and stable isotopic composition of living benthonic foraminifera and cold methane seep biogeochemistry in Monterey Bay: California, *Geochem. Geophys. Geosy.*, 4, 1106, doi:10.1029/2003GC000595, 2003.
- Reagan, M. T. and Moridis, G. J.: Oceanic gas hydrate instability and dissociation under climate change scenarios, *Geophys. Res. Lett.*, 34, L22709, doi:10.1029/2007GL031671, 2007.
- Reeburgh, W. S.: Oceanic methane biogeochemistry, *Chem. Rev.*, 107, 486–513, 2007.
- Reimer, P. J., Bard, E., Bayliss, A., Beck, J. W., Blackwell, P. G., Ramsey, C. B., Caitlin, E. B., Cheng, H., Edwards, R. L., Friedrich, M., Grootes, P. M., Guilderson, T. P., Haffidason, H., Hajdas, I., Hatté, C., Heaton, T. J., Hoffmann, D. L., Hogg, A. G., Hugen, K. A., Kaiser, K. F., Kromer, B., Manning, S. W., Niu, M., Reimer, R. W., Richards, D. A., Scott, E. M., Staff, R. A., Turney, C. S. M., and van der Plicht, J.: Intcal13 and Marine13 radiocarbon age calibration curves 0–50 000 years cal bp, *Radiocarbon*, 55, 1869–1887, 2013.
- Ritger, S., Carson, B., and Suess, E.: Methane-derived authigenic carbonates formed by subduction induced pore-water expulsion along the Oregon Washington margin, *Geol. Soc. Am. Bull.*, 98, 147–156, 1987.
- Sarnthein, M., Van Kreveld, S., Erlenkeuser, H., Grootes, P. M., Kucera, M., Pflaumann, U., and Schulz, M.: Centennial-to-millennial-scale periodicities of Holocene climate and sediment injections off the western Barents shelf, 75° N, *Boreas*, 32, 447–461, doi:10.1111/j.1502-3885.2003.tb01227.x, 2003.
- Sassen, R., Roberts, H. H., Carney, R., Milkov, A. V., DeFreitas, D. A., Lanoil, B., and Zhang, C.: Free hydrocarbon gas, gas hydrate, and authigenic minerals in chemosynthetic communities of the northern Gulf of Mexico continental slope: relation to microbial processes, *Chem. Geol.*, 205, 195–217, 2004.
- Screen, J. A. and Simmonds, I.: The central role of diminishing sea ice in recent Arctic temperature amplification, *Nature*, 464, 1334–1337, 2010.
- Sen Gupta, B. K. and Aharon, P.: Benthonic foraminifera of bathyal hydrocarbon vents of the Gulf of Mexico: initial report on communities and stable isotopes, *Geo-Mar. Lett.*, 14, 88–96, 1994.

- Sen Gupta, B. K., Platon, E., Bernhard, J. M., and Aharon, P.: Foraminiferal colonization of hydrocarbon-seep bacterial mats and underlying sediment, Gulf of Mexico slope, *J. Foramin. Res.*, 27, 292–300, 1997.
- Shakhova, N., Semiletov, I., Salyuk, A., Yusupov, V., Kosmach, D., and Gustafsson, Ö.: Extensive methane venting to the atmosphere from sediments of the East Siberian Arctic Shelf, *Science*, 327, 1246–1250, 2010.
- Shipley, T. H., Houston, M. K., Buffler, R. T., Shaub, F. J., McMullan, K. J., Ladd, J. W., and Worzel, J. L.: Seismic reflection evidence for the widespread occurrence of possible gas hydrate horizons on continental slopes and rises, *Am. Ass. Petrol. Geol. Bull.*, 63, 2201–2213, 1979.
- Sloan, E. D.: Gas hydrates: Review of physical/chemical properties, *Energy Fuels*, 12, 191–196, 1998.
- Smith, A. J., Mienert, J., Büinz, S., and Greinert, J.: Thermogenic methane injection via bubble transport into the upper Arctic Ocean from the hydrate-charged Vestnesa Ridge, Svalbard, *Geochem. Geophys. Geosy.*, 15, 1945–1959, doi:10.1002/2013GC005179, 2014.
- Smith, L. M., Sachs, J. P., Jennings, A. E., Anderson, D. M., and deVernal, A.: Light $\delta^{13}\text{C}$ events during deglaciation of the East Greenland continental shelf attributed to methane release from gas hydrates, *Geophys. Res. Lett.*, 28, 2217–2220, 2001.
- Smrzka, D., Kraemer, S. M., Zwicker, J., Birgel, D., Fisher, D., Kasten, S., Goedert, J. L., and Peckmann, J.: Constraining silica diagenesis in methane-seep deposits, *Palaeogeogr. Palaeoclimatol.*, 420, 13–26, 2015.
- Snyder, G. T., Hiruta, A., Matsumoto, R., Dickens, G. R., Tomaru, H., Takeuchi, R., Komatsubara, J., Ishida, Y., and Yu, H.: Pore water profiles and authigenic mineralization in shallow marine sediments above the methane-charged system on Umitaka Spur, Japan Sea, *Deep-Sea Res. Part II*, 54, 1216–1239, 2007.
- Spielhagen, R. F., Wermer, K., Aagaard-Sørensen, S., Zamelczyk, K., Kandiano, E., Budeus, G., Husum, K., Marchitto, T. M., and Hald, M.: Enhanced modern heat transfer to the Arctic by warm Atlantic water, *Science*, 331, 450–453, 2011.
- Stanford, J. D., Hemingway, R., Rohling, E. J., Challenor, P. G., Medina-Elizalde, M., and Lester, A. J.: Sea-level probability for the last deglaciation: A statistical analysis of far-field records, *Global Planet. Change*, 79, 193–203, 2011.
- Stuiver, M., Reimer, P. J., and Reimer, R. W.: CALIB Radiocarbon Calibration, Execute Version 7.0html, available at: <http://calib.qub.ac.uk/calib/> (last access: January 2015), 2014.
- Torres, M. E., Mix, A. C., Kinports, K., Haley, B., Klinkhammer, G. P., McManus, J., and de Angelis, M. A.: Is methane venting at the seafloor recorded by $\delta^{13}\text{C}$ of benthonic foraminifera shells?, *Paleoceanography*, 18, 1062, doi:10.1029/2002PA000824, 2003.
- Torres, M. E., Martin, R. A., Klinkhammer, G. P., and Nesbitt, E.: Post depositional alteration of foraminiferal shells in cold seep settings: New insights from flow-through time-resolved analysis of biogenic and inorganic seep carbonates, *Earth Planet. Sc. Lett.*, 299, 10–22, 2010.
- Treude, T., Boetius, A., Knittel, K., Wallmann, K., and Jørgensen, B. B.: Anaerobic oxidation of methane above gas hydrates at Hydrate Ridge, NE Pacific Ocean, *Mar. Ecol.-Prog. Ser.*, 264, 1–14, doi:10.3354/meps264001, 2003.
- Treude, T., Niggemann, J., Kallmeyer, J., Wintersteller, P., Schubert, C. J., Boetius, A., and Jørgensen, B. B.: Anaerobic oxidation of methane and sulfate reduction along the Chilean continental margin, *Geochim. Cosmochim. Ac.*, 69, 2767–2779, 2005.
- Vogt, P. R., Crane, K., Sundvor, E., Max, M. D., and Pfirman, S. L.: Methane-generated (?) pockmarks on young, thickly sedimented oceanic crust in the Arctic: Vestnesa ridge, Fram strait, *Geology*, 22, 255–258, 1994.
- Volkman, R. and Mensch, M.: Stable isotope composition ($\delta^{18}\text{O}$, $\delta^{13}\text{C}$) of living planktic foraminifers in the outer Laptev Sea and the Fram Strait, *Mar. Micropaleontol.*, 42, 163–188, 2001.
- Wallmann, P., Mahood, G., and Pollard, D.: Mechanical models for correlation of ring-fracture eruptions at Pantelleria, Strait of Sicily, with glacial sea-level drawdown, *Bull. Volcanol.*, 50, 327–339, 1988.
- Wefer, G., Heinze, P.-M., and Berger, W. H.: Clues to ancient methane release, *Nature*, 369, p. 282, 1994.
- Wollenburg, J. E., Kuhnt, W., and Mackensen, A.: Changes in Arctic Ocean paleoproductivity and hydrography during the last 145 kyr: The benthonic foraminiferal record, *Paleoceanography*, 16, 65–77, 2001.